We are IntechOpen,
the world's leading publisher of
Open Access books
Built by scientists, for scientists

6,900
Open access books available

186,000
International authors and editors

200M
Downloads

154
Countries delivered to

Our authors are among the

TOP 1%
most cited scientists

12.2%
Contributors from top 500 universities

CLARIVATE ANALYTICS
BOOK
CITATION
INDEX
INDEXED

WEB OF SCIENCE™

Selection of our books indexed in the Book Citation Index
in Web of Science™ Core Collection (BKCI)

Interested in publishing with us?
Contact book.department@intechopen.com

Numbers displayed above are based on latest data collected.
For more information visit www.intechopen.com

Steady-State Grain Size in Dynamic Recrystallization of Minerals

Ichiko Shimizu
Department of Earth and Planetary Science, University of Tokyo, Tokyo
Japan

1. Introduction

Dynamic recrystallization (DRX) is a strain restoration and grain refinement mechanism that occurs in high-temperature dislocation creep of metals and minerals (Humphreys & Hatherly, 2004). Microstructures indicative of DRX are commonly observed in rock-forming minerals that have been subjected to natural deformation in the Earth's crust and mantle (Fig. 1).

Laboratory studies have revealed that the average size d of recrystallized grains approaches a steady-state value, which is determined by the applied stress and is independent of the initial grain size. Twiss (1977) proposed a stress–grain size relation of the following form:

$$\frac{d}{b} = K \left(\frac{\sigma}{\mu} \right)^{-p} \tag{1}$$

where σ is the flow stress, μ is the shear modulus, b is the length of the Burgers vector, and K is a non-dimensional constant. The grain size exponent p ranges between 1 and 1.5 for most materials. Empirically determined σ–d relations of minerals have been used to estimate the stress states in the Earth's interior. However, detailed studies of a Mg alloy (De Bresser et al., 1998) and NaCl (Ter Heege et al., 2005) revealed that K has a weak dependence on temperature. Derby & Ashby (1987) modeled the DRX processes of metals and predicted the temperature dependence of the recrystallized grain size, but they failed to account for the observed range of exponent p (Derby, 1992; Shimizu, 2011).

In this chapter, we focus on deformation and recrystallization processes in minerals and examine the effects of stress and temperature on the steady-state grain size.

2. Recrystallization mechanisms in minerals

DRX was first observed in hot deformation of cubic metals such as Cu, Ni, and austenitic iron. A simplified description of DRX in these metals is as follows. Strain-free new grains are usually formed by bulging of pre-existing grain boundaries and they grow at the expense of old grains to reduce the dislocation energy of the material (Sakai, 1989; Sakai & Jones, 1984). As the dislocation density of the new grains increases, they cease to grow and new nucleation events occur at their margins. These processes repeat cyclically during dislocation creep.
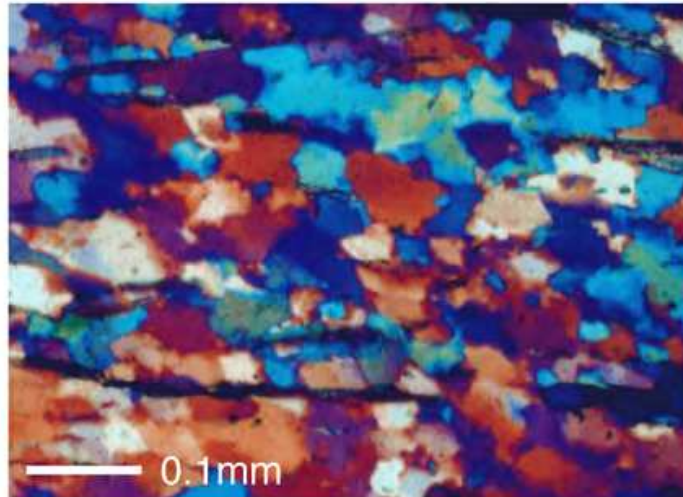
Fig. 1. Optical micrograph of a thin section of a quartz schist (Sanbagawa metamorphic belt, Japan) under polarized transmitted light with a sensitive color plate. Blue and red represent the orientation of the crystallographic *c*-axis of quartz grains. New small grains form at the margins and interiors of larger grains.

In contrast to the classical view of DRX described above, syndeformational recrystallization of minerals such as quartz, calcite, and olivine proceeds with progressive misorientation of subgrain boundaries (Poirier, 1985). Subgrain rotation (SGR) recrystallization also occurs in some metals such as Mg and Al alloys and is termed continuous DRX, whereas DRX in the original sense is currently referred to as discontinuous DRX (Humphreys & Hatherly, 2004). At low temperatures (T) and high strain rates ($\dot{\varepsilon}$), SGR is localized at grain margins (Hirth & Tullis, 1992; Schmid et al., 1980); however, intracrystalline SGR becomes more important and grain boundary migration (GBM) occurs at high T and low $\dot{\varepsilon}$ (Hirth & Tullis, 1992; Rutter, 1995) (Fig. 2). Consequently, the recrystallized grain size is much larger than the subgrain size (Guillopé & Poirier, 1979; Karato et al., 1980).

For both discontinuous and continuous DRX, grain size reduction occurs at nucleation events, whereas strain-induced GBM leads to overall coarsening. The steady-state grain size is determined by the dynamic balance between nucleation and grain growth (Derby & Ashby, 1987).

3. Grain size distribution

In the σ–d relation (Eq. 1), the steady-state microstructure is represented by a single value of the 'average' grain size d, but dynamically recrystallized materials generally have wide grain size distributions. As a simplified model of DRX, Shimizu (1998a; 1999; 2003) considered following nucleation and growth processes and analyzed the evolution of the grain size distribution:

1. Nucleation occurs at a constant rate I per unit volume.
2. Nucleation sites are randomly distributed.
3. Each grain grows with a radial growth rate $\dot{R}$.

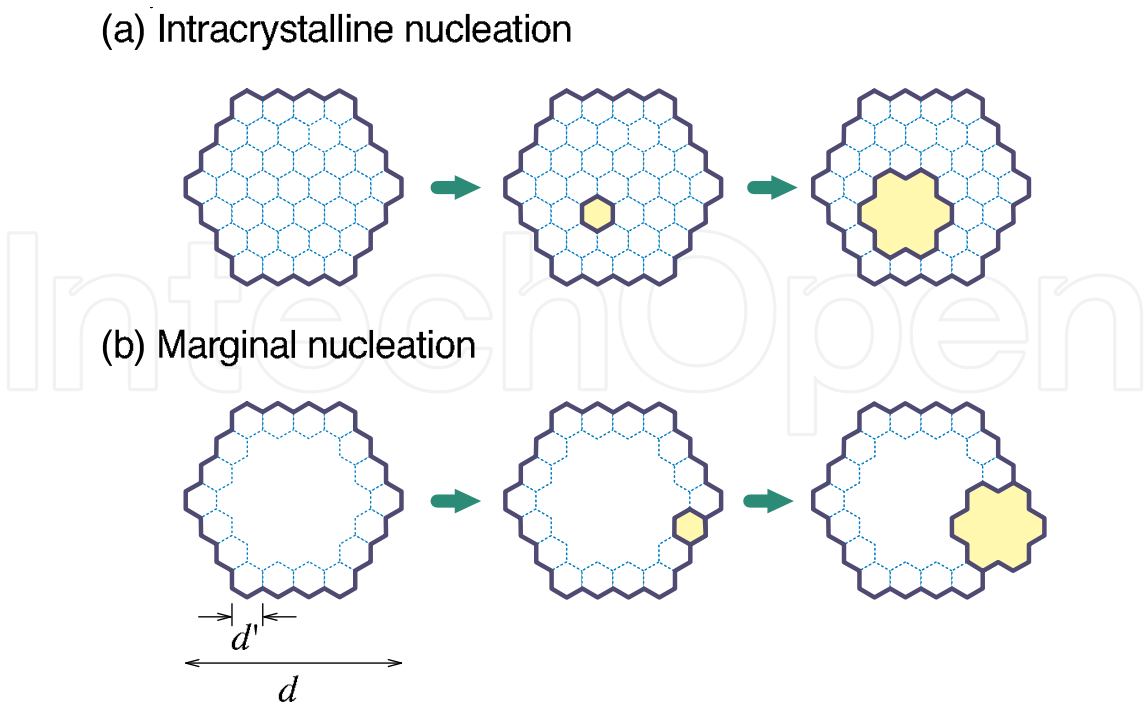## (a) Intracrystalline nucleation

(b) Marginal nucleation

Fig. 2. Nucleation and growth in continuous DRX. Solid lines represent grain boundaries and thin dotted lines represent subgrain boundaries. Nucleated grains (yellow) are formed by SGR and grow in the deformed matrix.

4. Newly crystallized grains replace older grains.

In the steady state, the grain size has a nearly a log-normal distribution and many newly crystallized grains coexist with a few old grains in a certain population balance. The average grain size satisfies

$$d = a \left(\frac{\dot{R}}{I} \right)^{\frac{1}{4}} \tag{2}$$

where a is a scaling factor; $a = 1.14$ for a 3D distribution and $a = 1.12$ for a distribution measured in a 2D section. Shimizu (1998b; 2008; 2011) considered strain-induced grain growth for $\dot{R}$ (Sec. 4) and SGR nucleation for I (Sec. 5) and derived the σ–d relation for continuous DRX (Sec. 6). In Sec. 7, we revise the theoretical model to incorporate the influence of the surface-energy drag.

4. Strain-induced grain growth

4.1 Dislocation energy

During high-T dislocation creep of minerals, dynamic recovery cooperates with continuous DRX and assists subgrain formation. Unrecovered microstructures such as tangled dislocations are rarely observed in recrystallized grains (Hirth & Tullis, 1992). Hence, the strain energy (E_{strain}) is given by a sum of the energies of isolated dislocations and sub-boundaries (E_{disl} and E_{sub}, respectively):

$$E_{strain} = E_{disl} + E_{sub} \tag{3}$$

The free dislocation energy per unit volume is

$$E_{disl} = \rho\zeta \tag{4}$$

where ρ is the dislocation density and ζ is the dislocation line tension. When the internal stress around dislocations is equilibrated with the applied stress σ, the following equation holds (Nabarro, 1987):

$$\sigma = \alpha\mu b\rho^{\frac{1}{2}} \tag{5}$$

where α is a constant that depends on the configuration of the dislocation arrays. Hence,

$$\rho = \left(\frac{\sigma}{\alpha\mu b}\right)^2 \tag{6}$$

The dislocation line tension is given by (Hirth & Lothe, 1982)

$$\zeta = \frac{\mu b^2 \chi}{4\pi}\ln\left(\frac{\beta r}{b}\right) \tag{7}$$

where r is the characteristic radius of the elastic field around the dislocation core and the constant β is typically in the range 3–4. The parameter χ depends on the dislocation configuration:

$$\begin{cases} \chi = 1; & \text{for a screw dislocation} \\ \chi = \dfrac{1}{1-\nu}; & \text{for an edge dislocation} \end{cases} \tag{8}$$

where ν is Poisson's ratio. For a first-order approximation, we assume that all dislocations are edge dislocations. Considering that the elastic field around a dislocation is canceled by other dislocations at half the distance between them, r is scaled as

$$r = \frac{1}{2}\rho^{-\frac{1}{2}} \tag{9}$$

Substituting Eqs. (6) and (9) into Eq. (7) yields

$$\zeta = \frac{\mu b^2}{4\pi(1-\nu)}\ln\left(\frac{\beta\alpha\mu}{2\sigma}\right) \tag{10}$$

Substituting Eq. (10) into Eq. (4) and using Eq. (6) again, we have

$$E_{disl} = \frac{\sigma^2}{4\pi\alpha^2\mu(1-\nu)}\ln\left(\frac{\beta\alpha\mu}{2\sigma}\right) \tag{11}$$

4.2 Sub-boundary energy

Consider nearly spherical subgrains with a diameter d' that occupy a deformed matrix (Fig. 2a). The number density of subgrains is

$$N = \frac{6}{\pi d'^3} \tag{12}$$

and the area of subgrain boundaries per unit volume is

$$A = N \cdot \pi d'^2 \cdot \frac{1}{2} = \frac{3}{d'} \tag{13}$$

The factor $1/2$ is included because the area of each subgrain wall is counted twice. The energy of sub-boundaries in a unit volume of the material can thus be written as

$$E_{sub} = \frac{3\gamma}{d'} \tag{14}$$

where γ is the sub-boundary energy per unit area.

The theory of dislocations gives

$$\gamma = \frac{\mu b^2}{4\pi(1-\nu)h}\xi(\eta) \tag{15}$$

$$\xi(\eta) \equiv \eta \coth \eta - \ln(2\sinh \eta) \tag{16}$$

$$\eta \equiv \frac{\pi b}{\beta h} \tag{17}$$

where h is the mean dislocation spacing (Hirth & Lothe, 1982).

For a tilt boundary (Fig. 3), h and the misorientation angle θ are related by (Poirier, 1985)

$$\frac{b}{h} = 2\tan\left(\frac{\theta}{2}\right) \simeq \theta \tag{18}$$

The last approximation is justified for low-angle boundaries. Then, Eq. (17) becomes

$$\eta = \frac{\pi}{\beta}\theta \ll 1 \tag{19}$$

Hence, the following approximations can be applied to Eq. (16):

$$\coth \eta \simeq \frac{1}{\eta}, \quad \sinh \eta \simeq \eta \tag{20}$$

Then, Eq. (15) becomes

$$\gamma = \frac{\lambda}{2}\mu b\theta \tag{21}$$

where

$$\lambda \equiv \frac{1}{2\pi(1-\nu)}\left[1 - \ln\left(\frac{2\pi\theta}{\beta}\right)\right] \tag{22}$$

The subgrain size is empirically expressed as (Takeuch & Argon, 1976; Twiss, 1977)

$$\frac{d'}{b} = K'\left(\frac{\sigma}{\mu}\right)^{-1} \tag{23}$$

where K' is a constant. A theoretical expression for K' is given below. Substituting Eqs. (21), (22), and (23) into Eq. (14), we have

$$E_{sub} = \frac{3\lambda\theta\sigma}{2K'} \tag{24}$$

4.3 Subgrain size

We consider a recovery process in which free dislocations with a dislocation density ρ rearrange into sub-boundaries. Conservation of the total dislocation length during subgrain formation requires

$$\rho = \frac{A}{h} \tag{25}$$

The right-hand side represents the length of dislocations in sub-boundaries. Using Eqs. (13) and (18), the above expression is modified to become

$$\rho = \frac{3\theta}{d'b} \tag{26}$$

Subgrains are formed if the total sub-boundary energy is smaller than the free dislocation energy (Twiss, 1977):

$$E_{disl} \geq E_{sub} \tag{27}$$

The equality represents the critical state for the initiation of subgrain formation. From Eqs. (4) and (14), this condition can be written as
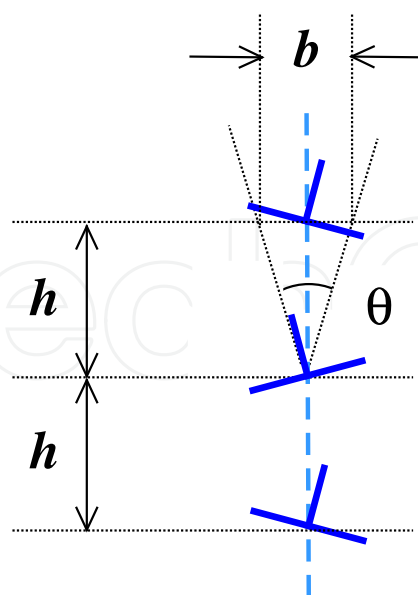
$$\rho\zeta \geq \frac{3\gamma}{d'} \tag{28}$$

Fig. 3. Schematic illustration of a tilt boundary with a misorientation angle θ, dislocation spacing h, and Burgers vector b.

Substituting Eqs. (6), (7), and (21)–(22) into the above expression for ρ, ζ, and γ, respectively, Eq. (28) becomes

$$\left(\frac{\sigma}{\alpha\mu b}\right)^2 b \ln\left(\frac{\beta\alpha\mu}{2\sigma}\right) \geq \frac{3}{d'}\theta\left[1 - \ln\left(\frac{2\pi\theta}{\beta}\right)\right] \tag{29}$$

Equating Eqs. (26) and (6), we have

$$\left(\frac{\sigma}{\alpha\mu b}\right)^2 = \frac{3\theta}{d'b} \tag{30}$$

Then, Eq. (29) reduces to

$$\ln\left(\frac{\beta\alpha\mu}{2\sigma}\right) \geq \left[1 - \ln\left(\frac{2\pi\theta}{\beta}\right)\right] \tag{31}$$

The stability limit of θ is derived as

$$\theta \geq \frac{e}{\pi\alpha}\left(\frac{\sigma}{\mu}\right) \tag{32}$$

where e is the Napierian base. The equality gives the initial misorientation angle θ_i:

$$\theta_i = \frac{e}{\pi\alpha}\left(\frac{\sigma}{\mu}\right) \tag{33}$$

Applying θ_i to θ of Eq. (30), the initial subgrain size d'_i is obtained as

$$\frac{d'_i}{b} = \frac{3e\alpha}{\pi}\left(\frac{\sigma}{\mu}\right)^{-1} \tag{34}$$

Once the subgrain boundary is established, it functions as a dislocation sink because progressive subgrain misorientation is an energetically favorable process. We thus assume that the subgrain size is maintained during the subsequent misorientation. Substituting $d' = d'_i$ into Eq. (34), we obtain Eq. (23), where

$$K' = \frac{3e\alpha}{\pi} \tag{35}$$

Using Eqs. (22) and (35), the full expression of Eq. (24) is obtained as

$$E_{sub} = \frac{\pi\lambda\theta\sigma}{2e\alpha} = \frac{\theta}{4e\alpha(1-\nu)}\left[1 - \ln\left(\frac{2\pi\theta}{\beta}\right)\right]\sigma \tag{36}$$

4.4 Growth kinetics

The kinetic law of grain growth is generally written as

$$\dot{R} = MF \tag{37}$$

where M is the mobility of the grain boundary and F is the driving force. M depends on T as
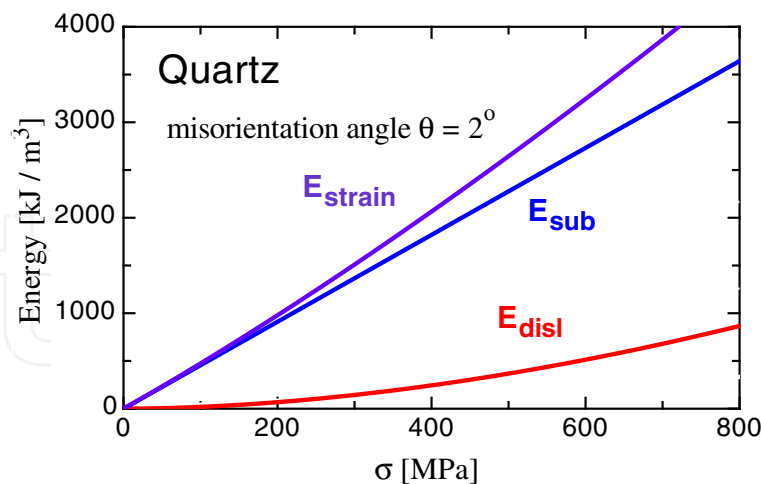
$$M = \frac{bwD_{gb}}{kT} \tag{38}$$

Fig. 4. Strain energy of quartz calculated using Eqs. (11) and (36). The physical parameters of quartz are given as (Shimizu, 2008) $\alpha = 3$ (Kohlstedt & Weathers, 1980), $\mu = 4.2 \times 10^4$ MPa, and $\nu = 0.15$ (Twiss, 1977). Because no data are available for β of quartz, we apply $\beta = 3$ of ionic crystals (Hirth & Lothe, 1982).

$$D_{gb} = D_{gb}^{\circ} \exp\left(-\frac{Q_{gb}}{RT}\right) \tag{39}$$

where w is the boundary width, k is the Boltzmann constant, D_{gb} is the diffusion coefficient at the grain boundary, D_{gb}° is a constant, R is the gas constant, and Q_{gb} is the activation energy for grain boundary diffusion.

In a single-phase material, grain growth occurs to reduce the bulk strain energy and the energy of grain surfaces. Hence, Eq. (37) is written as

$$\dot{R} = M(F_{strain} + F_{surf}) \tag{40}$$

where F_{strain} and F_{surf} represent the driving forces due to strain energy and surface energy (grain boundary energy), respectively. The strain energy in dynamically recrystallized materials is not homogeneous. The strain energy of deformed grains is given by the sum of E_{disl} in Eq. (11) and E_{sub} in Eq. (36), whereas newly recrystallized grains are almost strain free. This difference in strain energy drives grain growth. Hence,

$$F_{strain} = E_{strain} \tag{41}$$

With increasing strain, free dislocations multiply and excess dislocations rearrange into sub-boundaries. Then, θ increases and the sub-boundary energy exceeds the free dislocation energy. Fig. 4 shows the calculations for quartz. When the average misorientation angle reaches several degrees, the following approximation can be used instead of Eq. (3):

$$E_{strain} \simeq E_{sub} \tag{42}$$

5. Nucleation rate

In SGR nucleation, the nuclei are approximately the same size as the original subgrains. Thus, the number of potential nucleation sites per unit volume of crystals is given by Eq. (12) for intracrystalline nucleation and

$$N = \frac{6}{\pi d d'^2} \tag{43}$$

for nucleation at grain margins (Fig. 2b). The nucleation rate is scaled as

$$I = \frac{N}{\tau_c} \tag{44}$$

where τ_c is the interval of nucleation events.

The subgrain becomes a nucleus when the misorientation angle θ exceeds a critical value θ_c. The flux of dislocations that move toward the sub-boundary is given by ρu, where u is the climb velocity. The time required for dislocations to accumulate at the sub-boundary is equal to the nucleation cycle τ_c. From Eq. (18), a critical nucleus has a dislocation spacing of $h_c = b/\theta_c$; hence, the number of dislocations per unit area of the boundary is $1/h_c = \theta_c/b$. Dividing this value by the flux ρu, the nucleation cycle is evaluated as

$$\tau_c \simeq \frac{\theta_c}{b \rho u} \tag{45}$$

The climb velocity of dislocations is given by (Hirth & Lothe, 1982)

$$u = \frac{\sigma \Omega D_v}{lkT} \tag{46}$$

where Ω is the atomic volume, D_v is the self-diffusion coefficient, and l is a length scale given by

$$l \equiv \frac{b}{2\pi} \ln \left(\frac{r}{b} \right) \tag{47}$$

Using Eqs. (6) and (9), Eq. (47) can be rewritten as

$$l = \frac{b}{2\pi} \ln \left(\frac{\alpha \mu}{2\sigma} \right) \tag{48}$$

The temperature dependence of D_v is expressed as

$$D_v = D_v^\circ \exp \left(-\frac{Q_v}{RT} \right) \tag{49}$$

where D_v° is a constant and Q_v is the activation energy for volume diffusion.

Combining Eqs. (44)–(46), approximating Ω as b^3, and using Eqs. (12) and (23), we have

$$I = \frac{6}{\pi b K'^3 \alpha^2 \theta_c} \frac{\sigma D_v}{lkT} \left(\frac{\sigma}{\mu} \right)^5 \tag{50}$$

for intracrystalline nucleation. Using Eq. (43) instead of Eq. (12), the equation for marginal nucleation is obtained:

$$I = \frac{1}{d} \frac{6}{\pi K'^2 \alpha^2 \theta_c} \frac{\sigma D_v}{lkT} \left(\frac{\sigma}{\mu}\right)^4 \tag{51}$$

6. Scaling relation

Here, we neglect the surface energy term in Eq. (40) and assume

$$F = MF_{strain} \tag{52}$$

Combining Eq. (2) with Eqs. (52), (38), (39), (41), and (42), and using Eq. (36) and either Eq. (50) or Eq. (51), the steady-state grain size in continuous DRX is derived as

$$\frac{d}{b} = B \left(\frac{\sigma}{\mu}\right)^{-p} \left(\frac{wD_{gb}}{bD_v}\right)^{\frac{1}{m}} \tag{53}$$

where

$$p = \frac{5}{4} = 1.25, \ m = 4 \tag{54}$$

for intracrystalline nucleation and

$$p = \frac{4}{3} = 1.33, \ m = 3 \tag{55}$$

for marginal nucleation (Shimizu, 1998b; 2008). B is a non-dimensional constant given by

$$B = \left(\frac{a^4 \pi K'^{m-2} \alpha^2}{4} \frac{\lambda \theta \theta_c l}{b}\right)^{1/m} \tag{56}$$

Using Eq. (48), Eq. (56) can be rewritten as

$$B = \left[\frac{a^4 K'^{m-2} \alpha^2 \lambda \theta \theta_c}{8} \ln\left(\frac{\alpha \mu}{2\sigma}\right)\right]^{1/m} \tag{57}$$

Although σ is included in the right-hand side, the stress dependence of B is negligibly small. Using Eqs. (39) and (49), Eq. (53) can be re-expressed as

$$\frac{d}{b} = K^\circ \left(\frac{\sigma}{\mu}\right)^{-p} \exp\left(-\frac{\Delta Q}{mRT}\right) \tag{58}$$

where

$$K^\circ = B \left(\frac{wD_{gb}^\circ}{bD_v^\circ}\right)^{1/m} \tag{59}$$
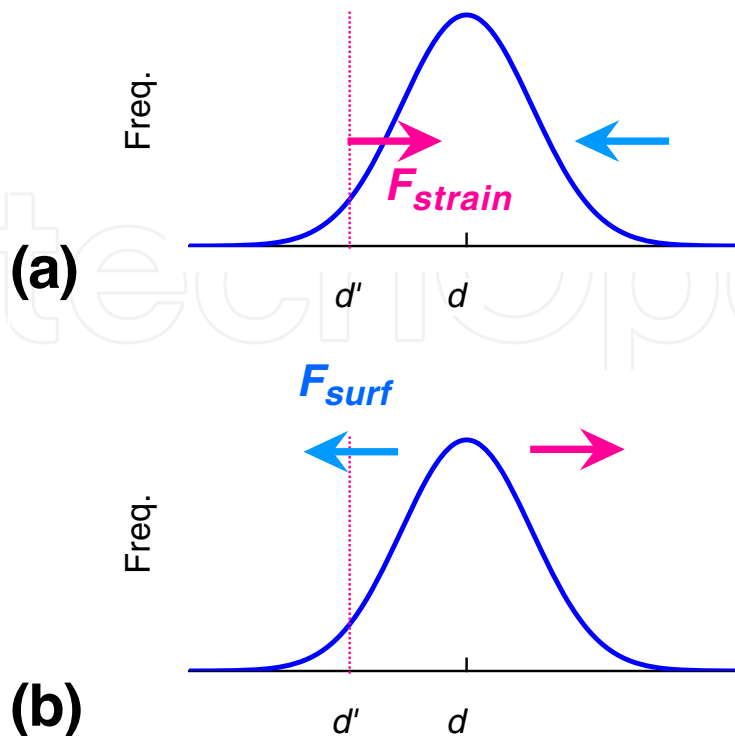
and

$$\Delta Q = Q_{gb} - Q_c \tag{60}$$

Fig. 5. Schematic representation of grain size evolution due to (a) strain-energy-driven grain growth and (b) surface-energy drag.

As Q_{gb} is generally smaller than Q_c, the recrystallized grain size is predicted to have a weak positive dependence on T. The constant K in Eq. (1) can now be written as a function of T:

$$K = K^\circ \exp\left(-\frac{\Delta Q}{mRT}\right) \tag{61}$$

7. Influence of surface energy

We now consider the influence of surface energy (grain boundary energy). In the case of surface-energy-driven grain coarsening in single-phase materials under static conditions (known as normal grain growth), large grains are energetically favorable and grow at the expense of small grains; the evolution of individual grain size has the opposite sense to that considered for DRX in Sec. 3 (Fig. 5). Therefore, when new grains grow by the strain-energy difference, the surface energy acts as a drag force.

In the theory of normal grain growth (Hillert, 1965), grain size evolution is described by

$$\dot{R}_k = Mc\Gamma\left(\frac{1}{R} - \frac{1}{R_k}\right) \tag{62}$$

where R_k and $\dot{R}_k$ are respectively the radius and the growth rate of the k-th grain and $c \sim 1$ is a statistical factor. If R_k is smaller (larger) than the mean radius R, the above expression becomes

negative and the k-th grain shrinks (grows). By comparison with Eq. (37), the driving force for the growth of the k-th grain can be written as

$$2c\Gamma \left(\frac{1}{d} - \frac{1}{d_k} \right) \tag{63}$$

where d_k is the diameter of the k-th grain. In the nucleation and growth processes in DRX, the influence of the surface-energy drag is largest for small nuclei. Thus, we introduce a modified factor c' and express the surface-energy-driven force in Eq. (40) as

$$F_{surf} = 2c'\Gamma \left(\frac{1}{d} - \frac{1}{d'} \right) \simeq -2c'\Gamma \frac{1}{d'} \tag{64}$$

With this equation and Eq. (42), Eq. (40) can be approximated as

$$\dot{R} \simeq M \left(E_{sub} - \frac{2c'\Gamma}{d'} \right) \tag{65}$$

Using this equation, Eq. (56) can be modified as follows (the parameters p, m, and ΔQ remain the same).

$$B = \left[\frac{a^4 K'^{m-2} \alpha^2 \theta_c}{8} \left(\frac{3\lambda\theta}{2} - \frac{2c'\Gamma}{b\mu} \right) \ln \left(\frac{\alpha\mu}{2\sigma} \right) \right]^{1/m} \tag{66}$$

8. Comparison of theory with experiments

8.1 Stress dependence of recrystallized grain size

In Fig. 6, p values of rock-forming minerals determined by triaxial or uniaxial or compression tests are plotted against the n-th power of dislocation creep flow laws ($\dot{\varepsilon} \propto \sigma^n$), which reflect the rate-controlling processes of dislocation creep; for climb-controlled creep, n is generally 3–5. The figure also shows the experimental result for a hexagonal Mg alloy (Magnox Al80), which was studied as a quartz analogue (De Bresser et al., 1998). The observed p values are almost independent of the power-law exponents and are well explained by the present model for continuous DRX.

8.2 Application to quartz

The theoretical model for the recrystallized grain size was applied to quartz using the equations presented in Sec. 6 (Shimizu, 2008; 2011). However, the previous model accounted only for strain energy; it neglected the effects of surface energy. Moreover, it turned out that the previous calculation involved a numerical error; when this error is corrected, the theoretical σ–d lines (Fig. 8 of Shimizu (2008)) shift to higher σ. Here, we recalculate the σ–d relation of quartz using the revised equations in Sec. 7.

Because experimentally deformed quartzite samples exhibit intracrystalline SGR at moderate stresses (Hirth & Tullis, 1992; Stipp & Tullis, 2003), we apply the intracrystalline nucleation model (Eq. 54). In addition to the material constants given in the caption of Fig. 4, we use $b = 5 \times 10^{-4}$ μm (Twiss, 1977), $\theta = 2°$, $\theta_c = 12°$, and D_v and D_{gb} of oxygen in β-quartz (Farver & Yund, 1991b; Giletti & Yund, 1984). For grain boundary energy, we use $\Gamma = 0.27$ Jm^{-2}
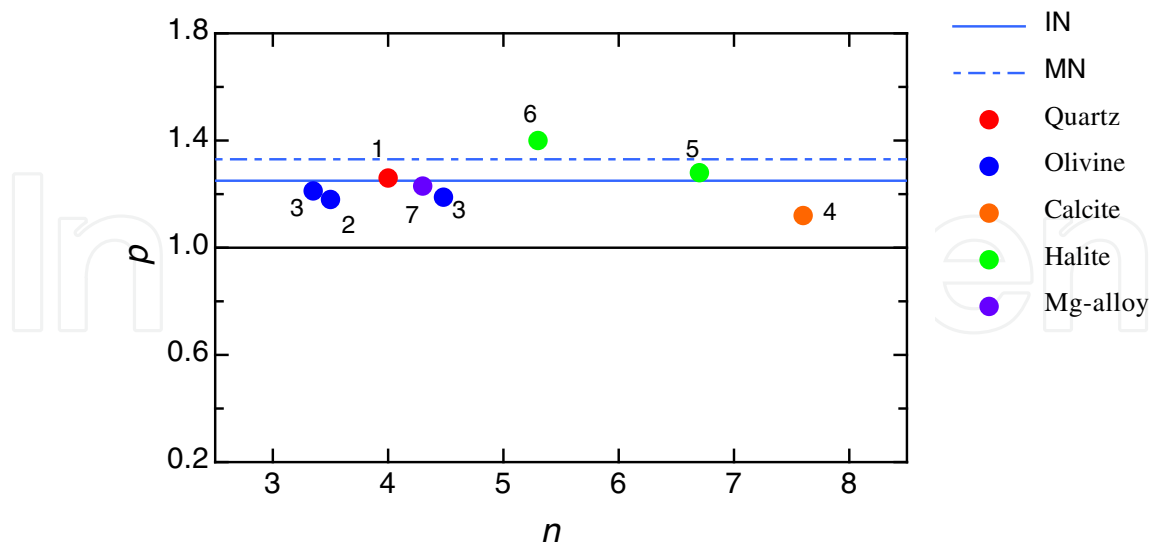
Fig. 6. Stress exponent p of recrystallized grain size plotted against the power-law exponent n of dislocation creep (IN: intracrystalline nucleation model; MN: marginal nucleation model). 1: Stipp & Tullis (2003) for p, Gleason & Tullis (1995) for n, 2: Karato et al. (1980) for p, Karato et al. (1986) for n, 3: van der Wal et al. (1993) for p, Chopra & Paterson (1984) for n, 4: Rutter (1995) for p, Schmid et al. (1980) for n, 5: Guillopé & Poirier (1979) for p and n, 6: Ter Heege et al. (2005) for p, Carter et al. (1993) for n, 7: De Bresser et al. (1998) for p and n. Microstructures of SGR and GBM are reported from all experiments except Ref. 3.

(Hiraga et al., 2007) and assume $c' = 1$. The steady-state grain size [μm] is then expressed a function of σ [MPa] and T [K] as

$$d = 1.82 \times 10^3 \times \sigma^{-1.25} \exp\left(\frac{7.25 \text{ kJ/mol}}{RT}\right) \quad ;\beta-\text{quartz} \tag{67}$$

In this expression, the weak stress dependence of B in Eq. (66) is neglected and $B = 1.01$ at σ=50 MPa is chosen as a representative value. The calculation results (Fig. 7a) agree well with the empirical data for β-quartz (Stipp & Tullis, 2003). For comparison, the σ–d relation based on the marginal nucleation model is also shown.

In Fig. 7(b), the theoretical model is extended to the α-quartz stability field in which D_v of oxygen in α-quartz (Farver & Yund, 1991a) is used and α- and β-quartz are assumed to have the same Q_v/Q_{gb} ratio. The recrystallized grain size of α-quartz is predicted to be

$$d = 9.98 \times 10^2 \times \sigma^{-1.25} \exp\left(\frac{12.4 \text{ kJ/mol}}{RT}\right) \quad ;\alpha-\text{quartz} \tag{68}$$

With decreasing temperature, the steady-state grain size shifts to higher stresses. If the empirical σ–d relation is directly applied to natural rocks that have deformed under low-T ($\leq 400°$C) metamorphic conditions, the stress states will be considerably underestimated.
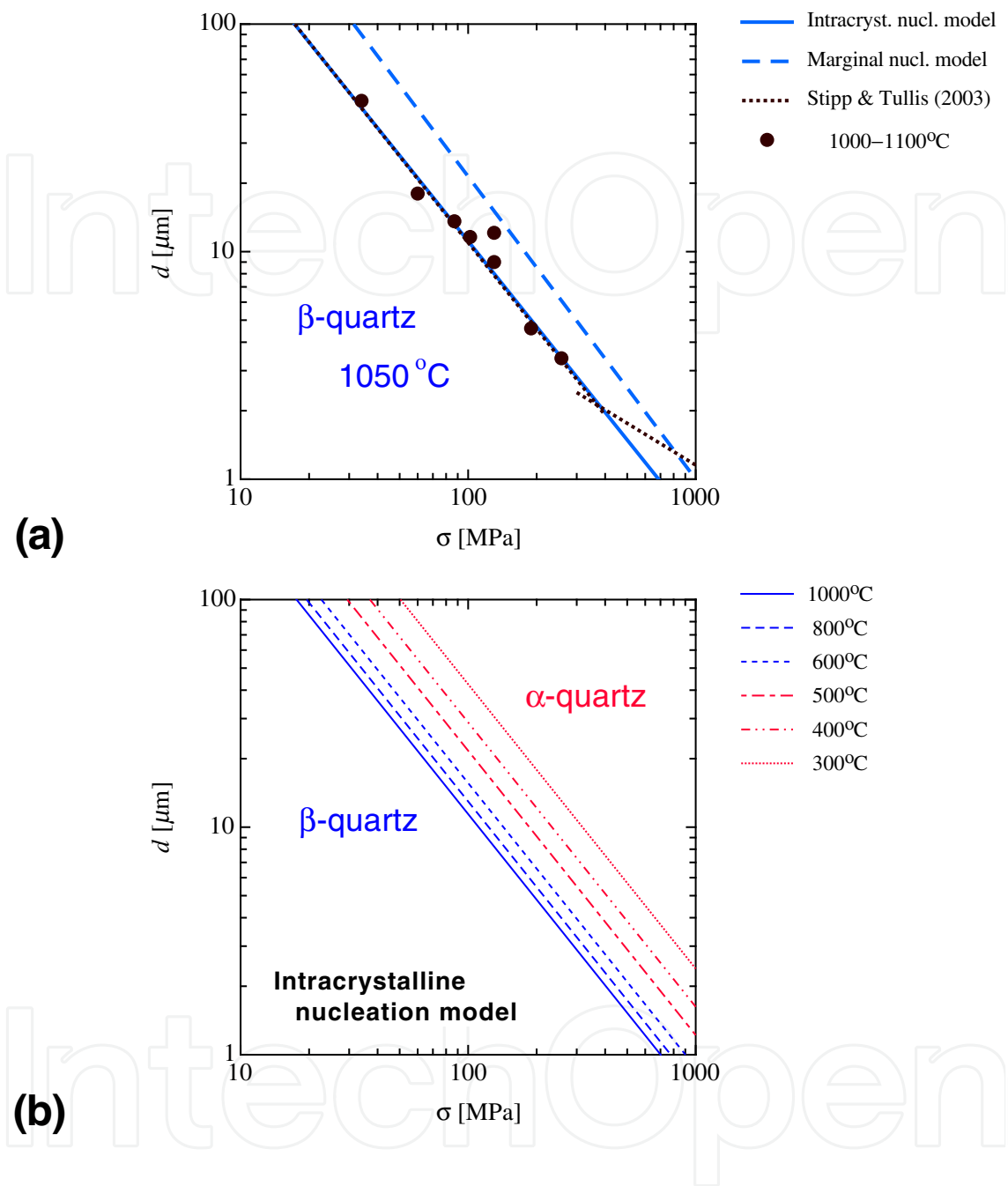
Fig. 7. Recrystallized grain size of quartz. (a) Theoretically calibrated σ–d relations for β-quartz at 1050°C and the experimental results of Stipp & Tullis (2003). Solid line: intracrystalline nucleation model. Dotted line: marginal nucleation model. Solid circles: recrystallized grain size at 1000–1100°C after Stipp & Tullis (2003). Black dotted line: empirical d–σ relation across the temperature range of 700–1100°C after Stipp & Tullis (2003). (b) Theoretically predicted σ–d relations for β-quartz (blue lines, 1000–600°C) and α-quartz (red lines, 500–300°C) using the intracrystalline nucleation model.
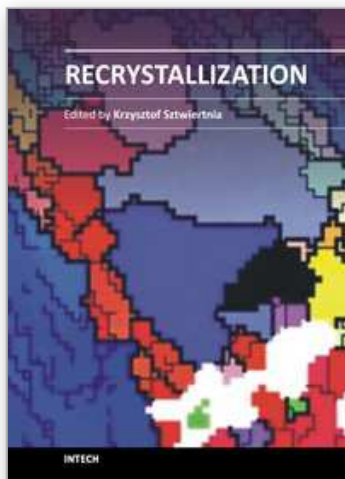
9. Summary

High-T dislocation creep of minerals is characterized by the occurrence of continuous DRX. The steady-state grain size is determined by the dynamic balance between SGR nucleation and grain growth by GBM. Surface energy acts as a drag force for strain-energy-driven GBM. The negative dependence of recrystallized grain size on stress is well explained by a theoretical model for continuous DRX. The theory also predicts a weak positive dependence of recrystallized grain size on temperature.

10. References

Carter, N.L.; Horseman, S.T.; Russel, J.E.; Handin, J. (1993). Rheology of rocksalt, *Journal of Structural Geology*, Vol. 15, 1257–1271.

Chopra P.N. & Paterson, M.S. (1984). The role of water in the deformation of dunite, *Journal of Geophysical Research* Vol. 89, 7861–7876.

De Bresser, J.H.P.; Peach, C.J.; Reijs, J.P.J.; Spiers, C.J. (1998). On dynamic recrystallization during solid state flow: effects of stress and temperature, *Geophysical Research Letters*, Vol. 25, 3457–3460.

Derby, B. (1992). Dynamic recrystallization: The steady state grain size, *Scripta Metallurgica and Materialia*, Vol. 27, 1581–1586.

Derby, B. & Ashby, M.F. (1987). On dynamic recrystallization, *Scripta Metallurgica*, Vol. 21, 879–884.

Farver, J. & Yund, R.A. (1991a). Oxygen diffusion in quartz: Dependence on temperature and water fugacity, *Chemical Geology*, Vol. 90, 55–70.

Farver, J. & Yund, R.A. (1991b). Measurement of oxygen grain boundary diffusion in natural, fine-grained, quartz aggregates, *Geochimica et Cosmochimica Acta*, Vol. 55, 1597–1607.

Gleason, G.C. & Tullis, J. (1995). A flow law for dislocation creep of quartz aggregates determined with the molten salt cell, *Tectonophysics*, Vol. 247, 1–23.

Giletti B.J. & Yund, R.A. (1984). Oxygen diffusion in quartz, *Journal of Geophysical Research*, Vol. 89, 4039–4046.

Guillopé, M. & Poirier, J.-P. (1979). Dynamic recrystallization during creep of single-crystalline halite: An experimental study, *Journal of Geophysical Research*, Vol. 84, 5557–5567.

Hillert, M. (1965). On the theory of normal and abnormal grain growth, *Acta Metallurgica*, Vol. 13, 227–238.

Hiraga, T.; Nishikawa, O.; Nagase, T.; Akizuki, M.; Kohlstedt, M. (2007). Interfacial energies for quartz and albite in pelitic schist, *Contributions to Mineralogy and Petrolgy*, Vol. 143, 663–672.

Hirth J.P. & Lothe J. (1982). *Theory of Dislocations*, Second edition, John Wiley & Sons, ISBN 0-471-09125-1, New York.

Hirth, G. & Tullis, J. (1992). Dislocation creep regimes in quartz aggregates, *Journal of Structural Geology*, Vol. 14, 145–159.

Humphreys, F.J. & Hatherly, M., (2004). *Recrystallization and Related Annealing Phenomena*, 2nd ed., Elsevier, ISBN 0-08-044164-5, Amsterdam.

Karato, S.; Paterson, M.S.; Fitz Gerald, J.D. (1986). Rheology of synthetic olivine aggregates: Influence of grain size and water, *Journal of Geophysical Research*, Vol. 91, 8151–8176.

Karato, S.; Toriumi, M.; Fujii, T. (1980). Dynamic recrystallization of olivine single crystals during high-temperature creep, *Geophysical Research Letters*, Vol. 7, 649–652.

Kohlstedt, D.L. & Weathers, M.S. (1980). Deformation-induced microstructures, paleopiezometers, and differential stress in deeply eroded fault zones, *Journal of Geophysical Research*, Vol. 85, 6269–6285.

Nabarro, F.R.N. (1987). *Theory of Crystal Dislocations*, Dover, ISBN 0-486-65488-5, New York.

Poirier, J.-P. (1985). *Creep of Crystals*, Cambridge University Press, ISBN 0-521-26177-5 (hardback) 0-521-27851 (paperback), Cambridge.

Rutter, E.H. (1995). Experimental study of the influence of stress, temperature, and strain on the dynamic recrystallization of Carrara marble, *Journal of Geophysical Research*, Vol. 100, 24651–24663.

Sakai, T. (1989). Dynamic recrystallization of metallic materials, In: *Rheology of solids and of the Earth*, Karato S. & Toriumi M. (Eds.), 284–307, Oxford University Press, ISBN 0-19-854497-9, Oxford.

Sakai, T. & Jonas, J.J. (1984). Dynamic recrystallization: mechanical and microstructural considerations, *Acta Metallurgica*, Vol. 32, 189–209.

Schmid, S.M.; Paterson, M.S.; Boland, J.N. (1980). High temperature flow and dynamic recrystallization in Carrara marble, *Tectonophysics*, Vol. 65, 245–280.

Stipp, M. & Tullis, J. (2003). The recrystallized grain size piezometer for quartz, *Geophysical Research Letters*, Vol. 30, 2088, doi:10.1029/2003GL018444.

Shimizu, I. (1998a). Lognormality of crystal size distribution in dynamic recrystallization, *FORMA*, Vol. 13, 1–11.

Shimizu, I. (1998b). Stress and temperature dependence of recrystallized grain size: A subgrain misorientation model, *Geophysical Research Letters*, Vol. 25, 4237–4240.

Shimizu, I. (1999). A stochastic model of grain size distribution during dynamic recrystallization, *Philosophical Magazine A*, Vol. 79, 1217–1231.

Shimizu, I. (2003). Grain size evolution in dynamic recrystallization. *Mater. Sci. Forum*, Vol. 426–432, Trans Tech Publ., Switzerland, 3587–3592.

Shimizu, I. (2008). Theories and applicability of grain size piezometers: The role of dynamic recrystallization mechanisms, *Journal of Structural Geology*, Vol. 30, 899–917.

Shimizu, I., (2011). Erratum to "Theories and applicability of grain size piezometers: The role of dynamic recrystallization mechanisms" [J Struct Geol 30 (2008) 899–917], *Journal of Structural Geology*, Vol. 33, 1136–1137.

Takeuchi, S. & Argon, A.S. (1976). Steady-state creep of single phase crystalline matter at high temperatures, *Journal of Materials Science*, Vol. 11, 1547–1555.

Ter Heege, J.H.; De Bresser, J.H.P.; Spiers, C.J. (2005a). Dynamic recrystallization of wet synthetic polycrystalline halite: dependence of grain size distribution on flow stress, temperature and strain, *Tectonophysics*, Vol. 396, 35–57.

Twiss, R.J. (1977). Theory and applicability of a recrystallized grain size paleopiezometer, *Pure and Applied Geophysics*, Vol. 115, 227–244.

van der Wal, D.; Chopra, P.; Drury, M.; Fitz Gerald, J. (1993). Relationships between dynamically recrystallized grain size and deformation conditions in experimentally deformed olivine rocks, *Geophysical Research Letters*, Vol. 20, 1479–1482.

Recrystallization

Edited by Prof. Krzysztof Sztwiertnia

Recrystallization shows selected results obtained during the last few years by scientists who work on recrystallization-related issues. These scientists offer their knowledge from the perspective of a range of scientific disciplines, such as geology and metallurgy. The authors emphasize that the progress in this particular field of science is possible today thanks to the coordinated action of many research groups that work in materials science, chemistry, physics, geology, and other sciences. Thus, it is possible to perform a comprehensive analysis of the scientific problem. The analysis starts from the selection of appropriate techniques and methods of characterization. It is then combined with the development of new tools in diagnostics, and it ends with modeling of phenomena.

How to reference

In order to correctly reference this scholarly work, feel free to copy and paste the following:

Ichiko Shimizu (2012). Steady-State Grain Size in Dynamic Recrystallization of Minerals, Recrystallization, Prof. Krzysztof Sztwiertnia (Ed.), ISBN: 978-953-51-0122-2, InTech, Available from: http://www.intechopen.com/books/recrystallization/steady-state-grain-size-in-dynamic-recrystallization-of-minerals

INTECH
open science | open minds